Shaped and Feedback-Controlled Excitation of Single Molecules in the Weak-Field Limit

Supporting Information

Alexander Weigel, Aleksandar Sebesta, Philipp Kukura*

Physical and Theoretical Chemistry Laboratory, University of Oxford

South Parks Road,

Oxford OX1 3QZ, United Kingdom

*philipp.kukura@chem.ox.ac.uk

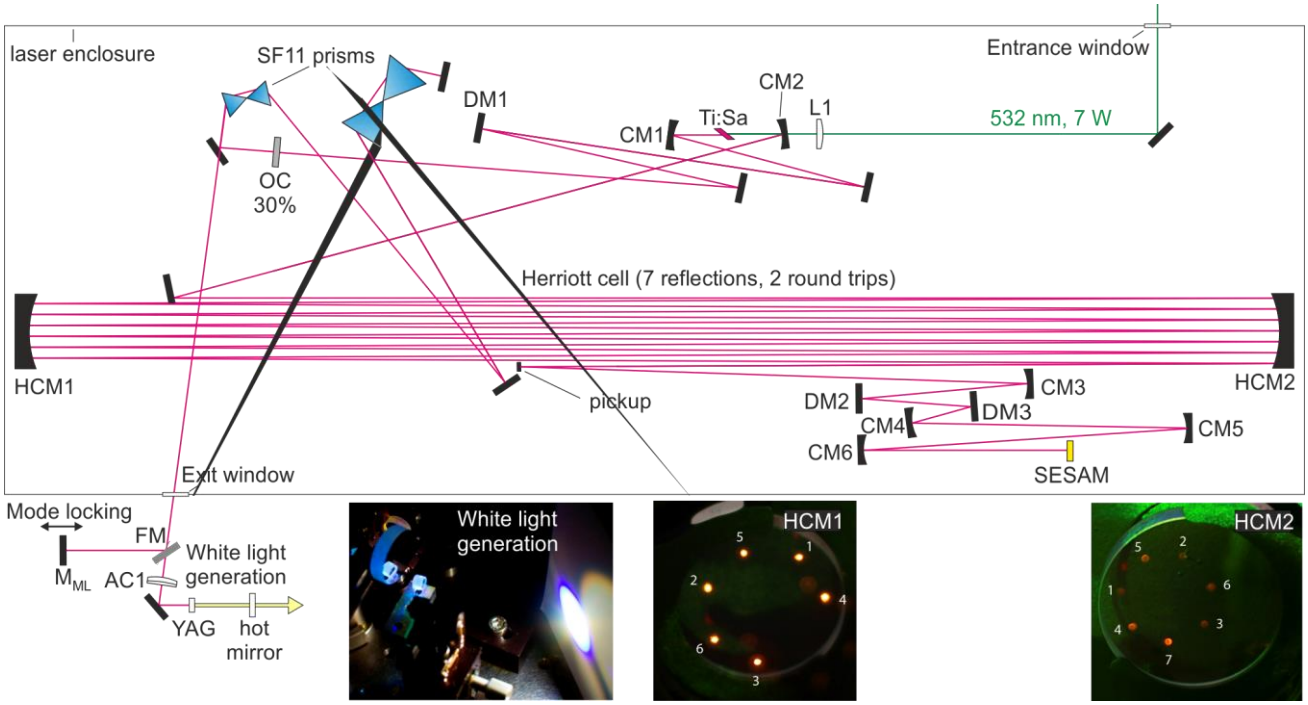

Supplementary Figure 1: Setup of the white light laser. The laser is based on a chirped pulse titanium:sapphire (Ti:Sa) oscillator, which is extended with a Herriott cell by 31.9 m round round trip length, thereby reducing the repetition rate to 8 MHz. The insets show the white light generation stage and the spot patterns at the Herriott cell mirrors HCM1 (r = -2 m) and HMC2 (r = -12 m). The laser is pumped by a 7 W Coherent Verdi G7 laser, focused with an f = 72 mm lens into the 3 mm thick Ti:Sa crystal. Mode locking is stabilized with a semiconductor saturable absorber mirror (SESAM, 3 % modulation depth), and intra-cavity dispersion is controlled with dispersion compensating mirrors (DM1: -50 fs^2 and DM2/3: mirror pair with -100 fs^2 each). After the 30 % output coupler (OC) the pulses are compressed with a 65 cm long double-SF11 prism compressor. The resulting pulses have a duration of 92 fs at 1.55 W output power corresponding to a pulse energy of 194 nJ. Mode-locking is started *via* the flip mirror FM by shaking the external mirror M_{ML}. An achromatic lens AC1 (f = 50 mm) focuses the laser output into a 4 mm thick YAG crystal to generate white light (see inset). A hot mirror removes the fundamental. The curved mirrors (CM) have the following radii: CM1 and CM2: -100 mm; CM3: -2 m; CM4: -300 mm; CM5: -200 mm; CM6: -400 mm.

Experimental Details

The 8 MHz White Light Source

Oscillators with repetition rates in the few-MHz regime provide an optimum duty cycle for single-molecule excitation, but are typically limited to the near infrared spectral range. Spectral coverage can now be routinely extended to the visible by white light generation in photonic crystal fibers,[1] but the output pulses have picosecond duration and are typically not compressible. We chose an alternative approach and generated femtosecond visible white light directly by focusing the output of a home-built high-power chirped pulse titanium:sapphire oscillator[2] into a YAG crystal (Supplementary Figure 1).

The oscillator is based on an asymmetric cavity with 120 cm and 60 cm arm lengths with two cavity mirrors of -100 mm radius, and a 30 % output coupler. The oscillator is pumped by the 7 W output of a Coherent Verdi G7 laser, focused with lens L1 (f = 72 mm) into the 3 mm thick titanium:sapphire crystal (Ti:Sa, Venteon). A Herriott cell consisting of two curved mirrors HCM1 (r = -2 m) and HCM2 (r = -12 m) at a separation of 1.14 m extends the short arm of the cavity by 31.9 m round trip length without affecting the optical properties,[2-4] and reduces thereby the repetition rate to 8 MHz, ideal for single-molecule experiments. At the Herriott cell mirrors a beam pattern of 7 spots with 2 round trips establishes (inset to Supplementary Figure 1). The last pass over HCM1 is replaced by a reflection at an external concave mirror CM3 of the same curvature. After the Heriott cell a mirror telescope reduces the beam diameter by a factor of 1.5 (CM4 and CM5), before another curved mirror, CM6 (r = -400 mm) focuses it onto a semiconductor saturable absorber mirror (SESAM, 3 % modulation). The combination of telescope and focusing mirror serves to adjust the fluence on the SESAM for optimum mode locking conditions. The cavity operates in the first stability regime, and in positive dispersion mode. Intra-cavity dispersion is controlled without any additional elements by the chirped mirrors DM1 (-50 fs^2

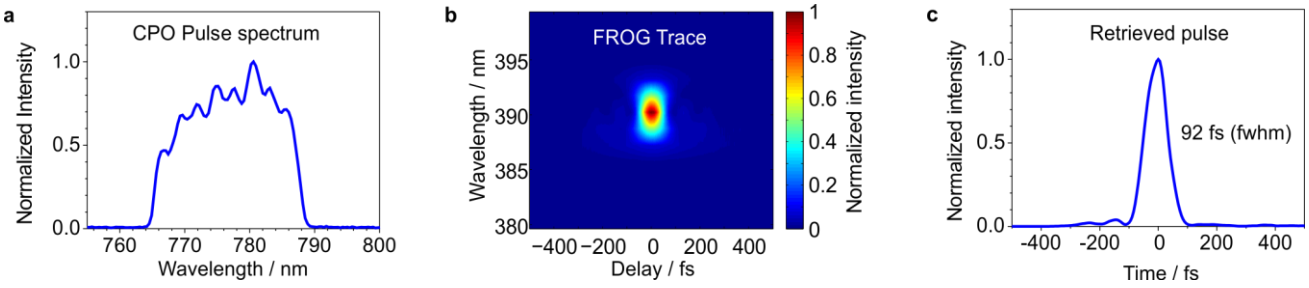

Supplementary Figure 2: Characterization of the chirped pulse oscillator (CPO) output after compression with the double SF11 prism compressor. **a** Typical output spectrum. **b** Second-harmonic frequency resolved optical gating (FROG) trace of the pulses. **c** Temporal pulse envelope retrieved from the FROG trace.

/ bounce) and DM2 / DM3 (-100 fs^2 / bounce, oscillation corrected) alone. In order to maximize mechanical stability, we mode locked the laser externally: The flip mirror FM closes an external cavity extension via mirror M_{ML}. The back-transmission into the cavity through the 30% output coupler is sufficient to mode-lock the laser by shaking M_{ML}. The mode-locked output is centred at 776 nm with a bandwidth of 22 nm. The strongly chirped output pulses are compressed with a 65 cm long double-SF11-prism compressor to 92 fs duration (see the FROG trace in Supplementary Figure 2 b, and the retrieved pulse envelope in panel c). The oscillator yields 1.55 W of compressed pulses with pulse energies of 194 nJ at 8 MHz repetition rate. All mirrors were supplied by Layertec and had a reflectivity of >99.9 % over the spectral range 720-850 nm, in which range they were also optimized for minimum GVD distortion.

As shown in the inset of Supplementary Figure 1, focusing the output of the chirped pulse oscillator with the achromatic lens AC1 (f = 50 mm) into a 4 mm thick YAG crystal generates visible white light.[5] The continuum spans a spectral region from 450 nm to the near infrared. A near-IR hot mirror (Thorlabs) removes the fundamental, leaving the spectrum in Supplementary Figure 3 a. The resulting pulses have a well-defined phase structure with mainly linear chirp and can be effectively compressed with standard techniques. Here, we use a pair of dispersion compensating mirrors (-40 fs^2 per reflection, Layertec) in combination with a pulse shaper to compress the pulses. The pulse duration is mainly limited by the spectral bandwidth of the shaping window, and we could obtain 7.5 fs pulses centered at 550 nm (blue in Supplementary Figure 3a and b). For the current experiments we truncated the spectrum to 470-595 nm, resulting in 10-12 fs pulse duration (magenta). The visible pulses have a power stability of 0.3 % rms over the duration of a typical experiment (Supplementary Figure 3 c). Over the duration of days SESAM deterioration impacts the laser performance, but slightly moving the illumination spot on the SESAM fully restores the original performance. The white light laser was routinely operated in this way on a daily basis over the duration of one year.

Pulse Characterization

We characterized the pulses with second-harmonic frequency-resolved optical gating (FROG). Since a reflective objective focused the excitation pulses onto the sample, no additional group velocity dispersion was

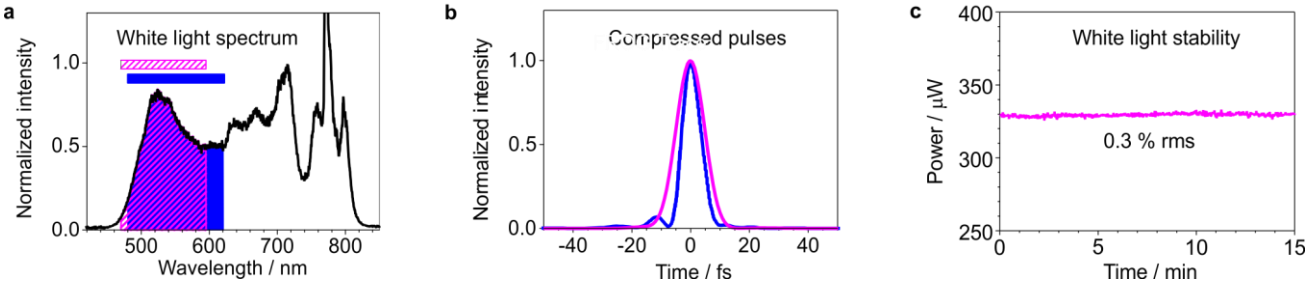

Supplementary Figure 3: Characteristics of the white light pulses. **a** White light spectrum after the near IR hot mirror. For the current experiments the we truncated the white light to the spectral range 470-595 nm (magenta); shorter pulses can be obtained for example with the blue band (480-622 nm). **b** Compressed pulses corresponding to the bands in a, as retrieved from experimental FROG traces. The pulse durations are 7.5 fs (blue) and 12 fs (magenta) full width of half maximum. **c** Power stability of the white light band marked in magenta.

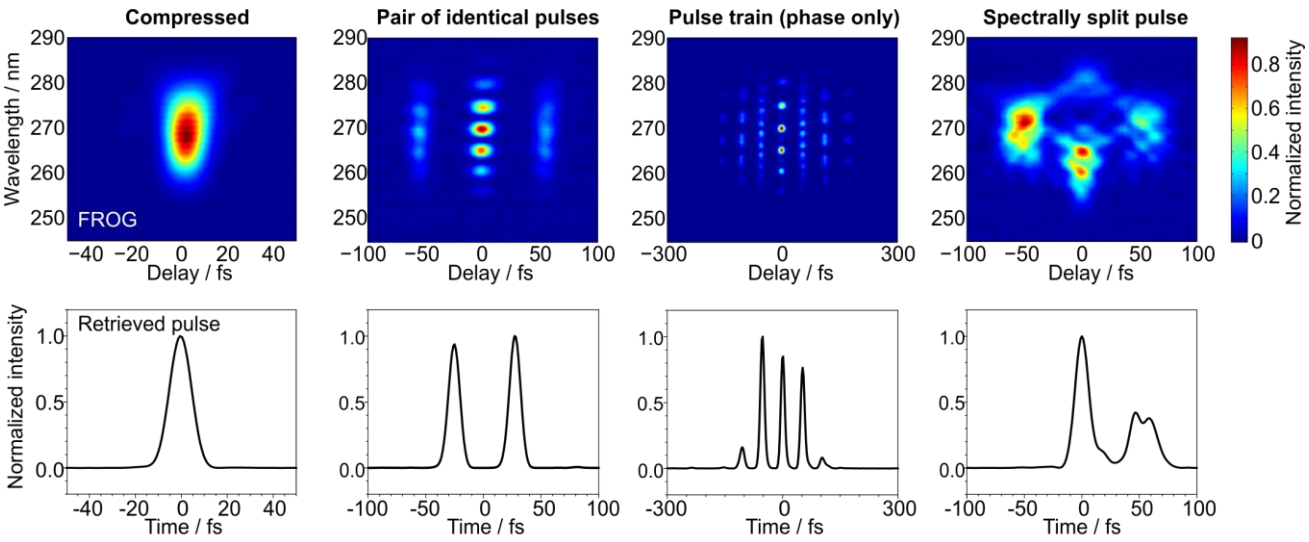

Supplementary Figure 4: Characterization of pulse shapes used to excite single terrylene molecules. Top row: Measured frequency resolved optical gating (FROG) traces. Bottom row: Temporal pulse profiles retrieved from the corresponding FROG traces. The FROG trace and retrieved pulse envelope in the first column correspond to the same measurement as in Supplementary Figure 3 (magenta).

introduced, and propagation effects do not influence single-molecule excitation.

The top row in Supplementary Figure 4 shows typical FROG traces for the pulse shapes used to excite the single terrylene molecules, with the retrieved temporal pulse structure underneath. The pulses were reconstructed with a Matlab algorithm provided by R. Trebino. For the compressed pulses we found durations of 10-12 fs without significant side bands. The difference to the transform limit (7.6 fs) is partly due to the chirped mirrors, which support only compression for wavelengths > 480 nm and may also be affected by the spectral response function of the FROG device.

In Supplementary Figure 4 we also characterize the multi-pulse sequences discussed in the main article, with 50 fs inter-pulse delay as an example. The generation of identical pulse pairs requires phase and amplitude shaping, whereas we created pulse trains and spectrally split pulses by phase-only shaping. The contrast of the retrieved pulses demonstrates that especially for pulse pairs and pulse trains the formation of satellites is negligible in the investigated delay range (0 ... 210 fs). The FROG trace of the spectrally split pulse exhibits some additional super-imposed modulation from phase-wrapping. Nonetheless, reconstruction yields two clearly separate pulses, which are broadened in time due to the reduced bandwidth.

Single Molecule Excitation

Supplementary Figure 5 presents a more detailed explanation of the downstream experimental setup. We used terrylene molecules embedded in a *p*-terphenyl matrix, a single-molecule system with extreme photostability, which can be illuminated under ambient conditions for several hours without photo-bleaching.[6] The aligned terrylene molecules were excited by directing the s-polarized excitation beam at an angle of 75 degrees onto the sample. Images of the dipole emission have a characteristic donut shape with an intensity minimum in the centre. [6-7] The single molecule image in Supplementary Figure 5 is the average over 3000 acquisitions with 100 ms exposure time each.

Background Correction

The single molecule images, which underlie the traces in Figures 1,2 and 3a/b of the main article contain a slight background signal. The faint lines in Supplementary Figure 5 indicate the wave guide nature of steps in the *p*-terphenyl matrix. The pure single molecule fluorescence was isolated by applying a 30-point 2-dimensional median filter and fitting the average donut shaped single-molecule image to each individual frame. The effectiveness of background rejection is evidenced in the Fourier transform spectra by (i) the lack

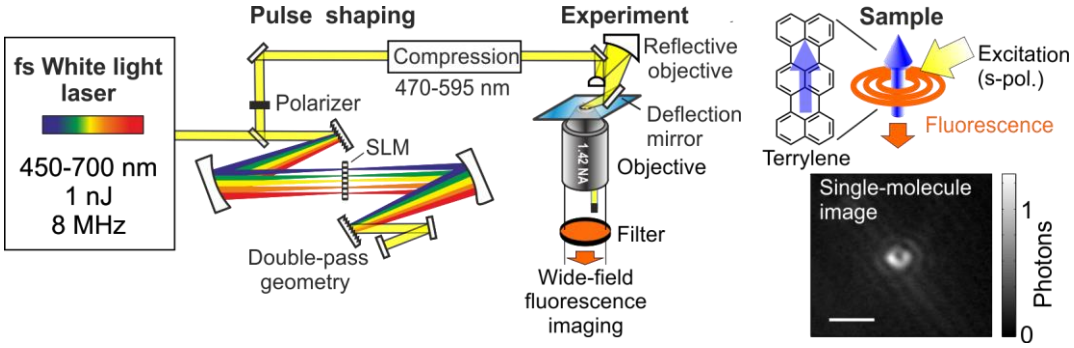

Supplementary Figure 5: Scheme of the experimental setup for coherent control experiments on single terrylene molecules. Visible femtosecond pulses from a white light laser with 8 MHz repetition rate were shaped in a grating-based 4f setup with a spatial light modulator (SLM), used in double pass geometry to avoid spatio-temporal coupling artefacts. Compression was accomplished with chirped mirrors. A reflective objective focused the s-polarized excitation beam via a deflection mirror at an angle of 75 degree onto the sample. In this way, the aligned single terrylene molecules with the transition dipole moment normal to the surface could be excited. The excitation power density was kept below 30-100 W/cm^2 The average fluorescence image (3000 acquisitions with 100 ms exposure) shows a donut shaped particle signal characteristic of dipole emission from the aligned molecules. Scale bar: 2 μm.

of a rising feature at the red edge of the spectra, which indicates that the obtained traces are not contaminated by excitation light bleeding through and (ii) the clarity of the obtained terrylene progression. For the closed-loop control experiments in Figure 3 c the background was suppressed experimentally with an additional 600 nm long pass filter (Thorlabs, FELH0600), so that the total single molecule fluorescence could be directly obtained by integrating over a 2.1 μm wide circular region of interest.

Confirmation that Single Molecules were Studied

It has been shown that isolated donut shaped fluorescence signals such as in Suppl. Fig. 5 are the images of single terrylene emitters with the transition dipole moments aligned normal to the glass surface.[6-7] Another direct evidence that individual terrylene molecules were studied is the single step bleaching in Supplementary Figure 6. The molecule in Suppl. Fig. 6 is the same as the one investigated in the pulse train experiment of Fig. 3a in the main article.

Fourier Transformation

Linear interference traces with $\Delta\phi = 0$ or $\Delta\phi = \pi$ are symmetric around zero delay. We acquired data in the range 0…210 fs. For the Fourier transformation in Figure 1d we zero-padded the signal to the range -420…420 fs and applied a Hann window before Fourier transformation. We applied here the Hann window after zero padding in order to retain the maximum information content, visible as fine structure in the absorption bands. The noise in this measurement is low enough that ringing from the finite signal step at $\pm$ 210 fs is small. The comparison experiments in Fig. 2 have lower signal/noise ratios, so that we apodized the signal first with a Hann window and zero-padded them then to the delay range -420 … 420 fs. As a result, the spectral features in Fig. 2c and d are slightly blurred compared to Fig. 1d.

The Genetic Algorithm

For closed loop optimization we adapted a Labview code for a genetic algorithm provided by the SLM manufacturer (Jenoptik) and incorporated several common strategies to improve convergence.

Population. The population of each generation consisted of 40 chromosomes, representing phase masks to be tested. The phase masks parameterized the SLM mask into 3.2 nm spaced phase values, which could vary freely between 0 and 2π with 5 bit precision, and were connected with cubic spline interpolation. The starting population consisted of random phase masks in the range 0 to 2π. The 10 best chromosomes of each generation survived without modification as part of the next generation. The other 30 chromosomes were modified by mutation and replaced by recombined chromosomes. This procedure was repeated for a given

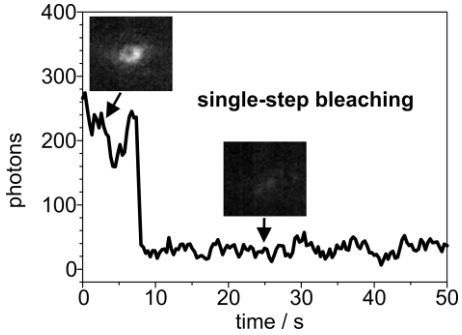

Supplementary Figure 6: Single-step bleaching of emission confirms that the donut-shaped fluorescence image corresponds to a single terrylene molecule. The molecule here is the same as the one studied in the pulse train experiment in the main article (Figure 3a).

number of generations. For a small number of phase masks (3.5 % in the optimization and 0.06 % in the de-optimization experiment) the interpolation produced unphysically large phase values, which could not be applied to the shaper. These individuals were discarded.

Fitness evaluation. We defined the fitness of a chromosome as the total signal with the individual phase mask to be tested relative to the signal of a spectrally flat reference phase mask. Multiple measurements were acquired for each individual chromosome to improve the signal/noise level. Since the convergence of the algorithm is driven by survival of the fittest and recombination of the best, we employed a selection round system to determine the fitness of the best performing chromosomes most precisely. In total we carried out 480 fitness measurements per generation. In a first round all 40 chromosomes were tested 3 times. An increasing number of additional measurements was then performed in consecutive rounds on the respective best individuals: 6 additional measurements on the best 20; then 12 additional measurements on the best 10, and finally 24 additional measurements on the best 5 chromosomes. The overall fitness was calculated from the average values of all test and reference measurements of each individual chromosome. As a consequence of the selection round system the best 5 chromosomes of a generation were tested 45 times, whereas the worst 20 chromosomes were only tested 3 times.

Selection. The chromosomes were ranked according to their fitness and the 30 best performing individuals were selected to create the next generation.

Survival of the fittest. The best 10 chromosomes entered the next generation directly without any modification.

Mutation. The remaining 20 chromosomes of the selection were mutated with a probability of 1. One of three operations was randomly performed:

(i) Each parameter mask was represented as a continuous 5 bit Gray code string, of which one bit was flipped.

(ii) The order of the parameters in a chromosome was rotated around a randomly chosen position. The new chromosome was then averaged with the original chromosome. This operation smoothed random fluctuations and shifts specific features to other spectral regions.

(iii) Each parameter was mapped into an integer representation in the range 1 to 2^5, and a randomly chosen single parameter of a chromosome was increased or decreased by one within this parameter range.

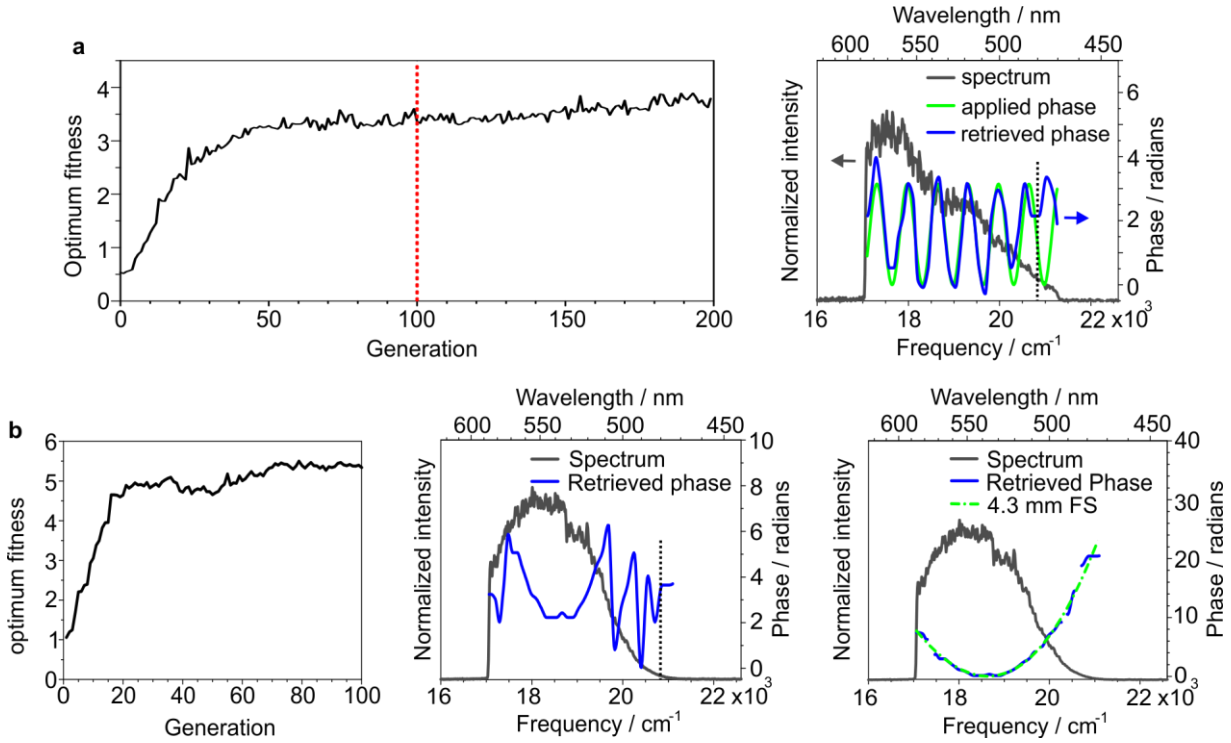

Supplementary Figure 7: Test of the genetic algorithm with the optimization of second harmonic generation. **a** Retrieval of an oscillatory phase applied to the SLM. Left: Convergence of the optimization. The dotted red line marks the number of generations in the single-molecule experiment. Right: Comparison of applied and retrieved phases. The dotted line indicates the spectral cut-off for compression with the chirped mirrors. **b** Retrieval of chirp from a 3 mm fused silica plate in the beam. Left: Convergence of the optimization. Middle: The retrieved phase describes the second-order phase distortion wrapped in the range 0 ... 2π. Right: The retrieved phase after unwrapping can be reproduced with the theoretical phase introduced by 4.3 mm fused silica. The difference in material thickness reflects the difficulty of the algorithm to wrap the phase with the relatively large 3.2 nm parameter spacing.

Recombination. Within the resulting selected individuals, genetic information was exchanged by recombination. 30 chromosome pairs were drawn within which two randomly selected segments were exchanged. One chromosome of each pair was then kept to form together with the 10 fittest and unchanged chromophores the population for the next generation.

Test of the Genetic Algorithm Performance

A typical application for the closed loop optimization with a genetic algorithm is the compression of femtosecond pulses with nonlinear signals as the feedback. We used the approach here with the second harmonic intensity of the pulse as the measured signal to evaluate the performance of the genetic algorithm. In a first experiment we applied a spectral phase oscillation to the compressed pulse, which produced a pulse train with 50 fs inter-pulse delay as shown in Supplementary Figure 4. Considering that the algorithm relies on random variation and the oscillation period is not uniform in the wavelength-linear space of the SLM, the phase mask pattern may be similar in complexity to the solution we sought in the single molecule experiment. Supplementary Figure 7a shows the experimentally determined fitness of the best chromosome of each generation. The algorithm has almost completely converged after 40 generations with only minor improvement thereafter. Accordingly, significant convergence should be expected even for complicated pulse shapes after optimization over 100 generations (red line) as in the single molecule experiment. The negative of the optimal compression phase retrieved the originally applied phase oscillation within the spectral range of the chirped mirrors, which is limited to below 480 nm (dotted line).

In a second experiment we chirped the compressed pulses with 3 mm fused silica in the beam. The genetic algorithm converges in this experiment very quickly, already within 20 generations (Supplementary Figure 7b, left). The available phase range from 0 to 2π does not cover the full range of the phase distortion, so the retrieved phase is wrapped (Supplementary Figure 7, middle). In Supplementary Figure 7, right, we have

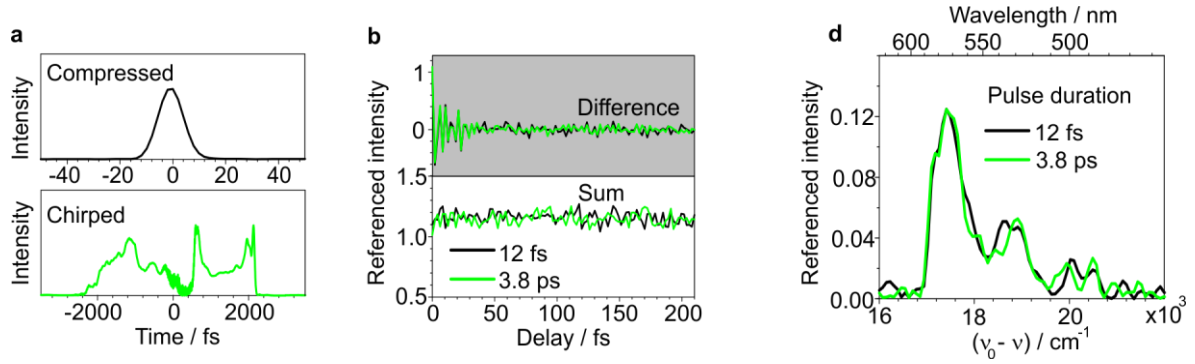

Supplementary Figure 8: The effect of pulse duration on the single molecule fluorescence modulation in a pulse pair experiment. Results underlying Figure 2d in the main article. **a** Retrieved compressed and chirped pulse envelopes. **b** Difference and sum fluorescence traces. **c** Fourier transform spectra as in the the main article.

unwrapped the phase and omitted the intermediate parts. The resulting curve has the parabolic shape characteristic for linear chirp, and is reproduced theoretically by the phase distortion introduced by 4.3 mm fused silica. The difference in experimentally applied and retrieved material thickness reflects the incomplete phase wrapping due to the relatively large, 3.2 nm, spacing of the parameter mask. Nonetheless, the algorithm efficiently converges to a compromise solution, which maximizes the second harmonic generation. Note that the phase wrapping for the split pulse experiment in Figure 3b is more accurate, since there the 2π phase steps occur between two pixels of the shaper mask, which are only 0.4 nm apart.

Effect of Pulse Duration on a Pulse Pair Experiment: Additional Results

Supplementary Figure 8a shows the retrieved temporal profiles of the compressed and chirped pulses used in the experiment presented in Figure 2d. The difference and sum delay traces (Supplementary Figure 8b) demonstrate also in time domain that stretching the pulse to 3.8 ps does not affect the single molecule fluorescence behaviour in this experiment. Inverse Fourier transformation of the difference trace yields then the fluorescence excitation spectra (Supplementary Figure 8c) already presented in Figure 2d in the main article. The phase locking for this experiment was set to ν_0 = 23,810 cm^{-1} (420 nm).

Single-Molecule Weak-Field Excitation in the Liouville Picture

For further discussion consider the Liouville pathways in Supplementary Figure 9. Spontaneous luminescence can be described by two electric field interactions with the excitation field and two electric field interactions with the vacuum field.[8] Sequential paths describe fluorescence, whereas the coherent interaction of excitation and vacuum fields generates the much weaker spontaneous Raman signal, which can be neglected here. We distinguish two different types of wave packets in the absorption process.

Two electric field interactions with a broadband femtosecond pulse leave the molecule in a coherent vibrational superposition state of the Franck-Condon active stretching mode in the excited state. The wave packet will roam on the potential energy surface of the excited state, and mediated by interaction with the environment, the phase of the incident pulse could in principle steer the wavepacket towards a region on the potential energy surface with enhanced or decreased internal conversion probability to the ground state. However, our results demonstrate that also such effects do not play a role here. Spontaneous emission occurs randomly in time, so that the experimental acquisition intrinsically averages over any time-dependent information. Therefore we cannot follow the motion of the vibrational wave packet in a linear pulse pair experiment without the existence of additional control channels, although in the nonlinear regime a photon from the second pulse may dump the initially prepared wave packet at a specific delay time down to the ground state and thereby track its motion.[9] These types of vibrational wavepackets have been produced and studied over the past decades in various implementations of nonlinear ultrafast spectroscopy.[10-13] Our results suggest also that – at least for systems such as ours – it is not possible to change the non-radiative internal conversion rate by driving the wavepacket with tailored pulse shapes into a specific direction.

A single interaction with the excitation field prepares the system in a superposition of ground and excited electronic states, which can be considered a vibronic wavepacket. Absorption of a photon can be described in this picture as the interference of an evolved vibronic wavepacket from the first excitation field interaction with

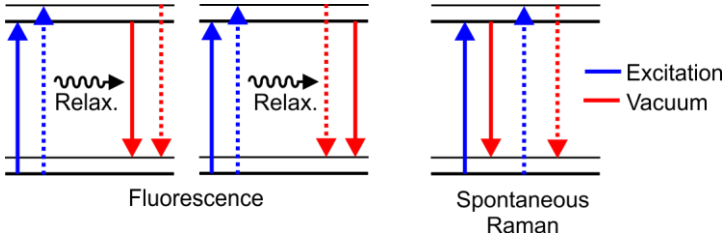

Supplementary Figure 9: Liouville pathways contributing to spontaneous luminescence. The molecule interacts twice with the excitation electric field and twice with the vacuum electric field. Full arrows represent interaction on the bra side, dashed arrows on the ket side. Sequential pathways describe fluorescence, whereas the coherent interaction of pump and vacuum fields leads to weak spontaneous Raman scattering.

another vibronic wavepacket launched by the second excitation field interaction.[14] The evolution of the wavepacket on the excited state determines the shape of the absorption spectrum. The homogeneous linewidth of terrylene is at room temperature much broader than at cryogenenic temperatures, demonstrating that interaction with the bath is responsible for truncating the electronic coherence after excitation.[15] The phase of the excitation pulse could in principle affect the truncation and alter, whether the collapse of the electronic coherence results in electronic excitation or not, leading in the long-term limit to a change in the time-averaged fluorescence intensity. The decay of the oscillations in Figure 2b suggests that electronic dephasing takes for our system ca. 50 fs, so that the 12 fs excitation pulses are sufficiently short to specifically interact in time with the vibronic wavepacket. However, our results suggest that the wave packet motion is controlled solely by the intrinsic natural properties of the molecular system and is in the one photon limit not modified by the phase of the electric field. Any control through the electric field reduces here to changes in its spectral content.

References

(1) Russell, P., Photonic Crystal Fibers. *Science* **2003,** *299*, 358-362.
(2) Fernandez, A.; Fuji, T.; Poppe, A.; Fürbach, A.; Krausz, F.; Apolonski, A., Chirped-Pulse Oscillators: A Route to High-Power Femtosecond Pulses without External Amplification. *Opt. Lett.* **2004,** *29*, 1366-1368.
(3) Kowalevicz, A. M.; Sennaroglu, A.; Zare, A. T.; Fujimoto, J. G., Design Principles of Q-Preserving Multipass-Cavity Femtosecond Lasers. *J. Opt. Soc. Am. B* **2006,** *23*, 760-770.
(4) Siegel, M.; Pfullmann, N.; Palmer, G.; Rausch, S.; Binhammer, T.; Kovacev, M.; Morgner, U., Microjoule Pulse Energy from a Chirped-Pulse Ti:Sapphire Oscillator with Cavity Dumping. *Opt. Lett.* **2009,** *34*, 740-742.
(5) Bradler, M.; Baum, P.; Riedle, E., Femtosecond Continuum Generation in Bulk Laser Host Materials with sub-µJ Pump Pulses. *Appl. Phys. B* **2009,** *97*, 561-574.
(6) Pfab, R. J.; Zimmermann, J.; Hettich, C.; Gerhardt, I.; Renn, A.; Sandoghdar, V., Aligned Terrylene Molecules in a Spin-Coated Ultrathin Crystalline Film of *p*-Terphenyl. *Chem. Phys. Lett.* **2004,** *387*, 490-495.
(7) Lee, K. G.; Chen, X.W.; Eghlidi, H.; Kukura, P.; Lettow, R.; Renn, A.; Sandoghdar, V.; Götzinger, S., A Planar Dielectric Antenna for Directional Single-Photon Emission and Near-Unity Collection Efficiency. *Nature Photon.* **2011,** *5*, 166-169.
(8) Mukamel, S., *Nonlinear Spectroscopy*. Oxford University Press: Oxford, 1995.
(9) Westphal, V.; Kastrup, L.; Hell, S., Lateral Resolution of 28 nm (Lambda/25) in Far-field Fluorescence Microscopy. *Appl. Phys. B* **2003,** *77*, 377-380.
(10) Zewail, A. H., Femtochemistry: Atomic-Scale Dynamics of the Chemical Bond. *J. Phys. Chem. A* **2000,** *104*, 5660-5694.
(11) Huxter, V. M.; Over, T. A. A.; Budker, D.; Fleming, G. R., Vibrational and Electronic Dynamics of Nitrogen-vacancy Centers in Diamond Revealed by Two-dimensional Ultrafast Spectroscopy. *Nature Phys.* **2013,** *9*, 744-749.
(12) Kraack, J. P.; Wand, A.; Buckup, T.; Motzkus, M.; Ruhman, S., Mapping Multidimensional Excited State Dynamics Using Pump-Impulsive-Vibrational-Spectroscopy and Pump-Degenerate-Four-Wave-Mixing. *Phys. Chem. Chem. Phys.* **2013,** *15*, 14487-14501.
(13) Liebel, M.; Kukura, P., Broad-Band Impulsive Vibrational Spectroscopy of Excited Electronic States in the Time Domain. *J. Phys. Chem. Lett.* **2013,** *4*, 1358-1364.

(14) Heller, E. J., The Semiclassical Way to Molecular Spectroscopy. *Acc. Chem. Res.* **1981,** *14*, 368-375.
(15) Kummer, S.; Kulzer, F.; Kettner, R.; Basche, T.; Tietz, C.; Glowatz, C.; Kryschi, C., Absorption, Excitation, and Emission Spectroscopy of Terrylene in p-Terphenyl: Bulk Measurements and Single Molecule Studies. *J. Chem. Phys.* **1997,** *107*, 7673-7684.